

Radiation hardness study on a CMOS pixel sensor for charged particle tracking

L. Li,^a L. Zhang,^{a,1} J. N. Dong,^a J. Liu,^b M. Wang^{a,1}

*Institute of Frontier and Interdisciplinary Science and Key Laboratory of Particle Physics and Particle Irradiation, Shandong University,
Qingdao, 266237, Shandong, China*

^b*Department of Physics, University of Liverpool, Liverpool, L693BX, United Kingdom*

E-mail: mwang@sdu.edu.cn, zhang.1@sdu.edu.cn

ABSTRACT: A CMOS pixel sensor, named SUPIX-1, is developed for a pixelated silicon tracker for the Circular Electron-Positron Collider (CEPC) project. The sensor, consisted of nine sectors varying in pixel sizes, diode sizes and geometries, is fabricated with a 180 nm CMOS Image Sensor (CIS) process to study the particle detection performance of enlarged pixels. In this work, the radiation-induced effects on the charge collection of the sensor under the fluence of 1×10^{13} 1 MeV n_{eq}/cm^2 are studied by the measurements with the radioactive source of ^{55}Fe and the Technology Computer Aided Design (TCAD) simulations, since the radiation hardness of 6.8×10^{12} 1 MeV n_{eq}/cm^2 per year for Non-Ionizing Energy Loss (NIEL) effects is required. In measurements, the sensor gain has been calibrated using the $k\alpha$ peak of ^{55}Fe before and after irradiation. The pixel-wise equivalent noise charge (ENC), charge collection efficiency (CCE) and signal-to-noise ratio (SNR) were evaluated. The radiation-induced effects on cluster properties are studied through a self-developed reconstruction algorithm. In TCAD simulations, charge collections in 5×5 pixel matrixes for two typical impinging cases of incident particles were simulated with and without irradiation. Both measurements and simulations indicate that enlarged pixels with area of $21 \mu m \times 84 \mu m$, though suffering greater loss on sensor performance than small pixels do, still have satisfactory noise and charge collection performance after irradiation for particle tracking in the upcoming collider detectors.

KEYWORDS: CMOS imagers, Particle tracking detector and programs, TCAD, Radiation-hard detectors

ARXIV EPRINT: [1234.56789](https://arxiv.org/abs/1234.56789)

¹Corresponding author.

Contents

| | | |
|----------|--|----------|
| 1 | Introduction | 1 |
| 2 | Measurements with ^{55}Fe | 2 |
| 2.1 | The sensor gain calibration | 3 |
| 2.2 | The cluster-wise sensor properties | 5 |
| 3 | TCAD simulations | 7 |
| 4 | Conclusion | 9 |

1 Introduction

A CMOS pixel sensor, named Shandong University PIXel (SUPIX-1), is developed for silicon tracker of CEPC[1, 2] for precision tracking. Shown in Figure 1(a), the sensor chip covers a sensitive area of $2 \times 8 \text{ mm}^2$ containing 9 sectors (A0-A8). Each sector contains 64 rows and 16 columns of pixels. Three pixel pitches and six sets of diode geometries are implemented in the sensor, whereas five sectors are functional in the test (A0, A2, A5, A7 and A8). The sensitive area, the pixel pitch and the diode geometry for corresponding sectors are listed in Table 2. The diode surface is defined as the area of N-well and the diode footprint is the area surrounded by P-well, shown in Figure 1(b). Additionally, a staggered pixel design, shown in Figure 1(c), is implemented in sectors with large x-pitch ($84 \mu\text{m}$) to enhance the charge collection. Details of the pixel design can be found in ref. [3].

The radiation hardness of bulk damage on sensors, scaled with the NIEL[4], is important for the operations of pixelated tracking devices in a collider environment. The main effects on macroscopic sensor properties are[4, 5]

- Increase of the leakage current.
- Increase of the biasing voltage on diode needed to achieve a given thickness of the active area. In other words, the depleted region gets thinner with the same biasing conditions.
- Charge trapping due to defects, which reduce the charge collection efficiency.

A value of $6.2 \times 10^{12} \text{ 1 MeV n}_{\text{eq}}/\text{cm}^2$ for the NIEL per year is estimated for the first layer of CEPC vertex detector[2]. Thus, the SUPIX-1 sensor has been irradiated under the fluence of $1 \times 10^{13} \text{ 1 MeV n}_{\text{eq}}/\text{cm}^2$ at China Spallation Neutron Source (CSNS) to study the radiation-induced effects on sensor performance. The measurements of the sensor performance with the radioactive source of ^{55}Fe before and after irradiation are demonstrated in Section 2. The test results, taking A0 as an example, are discussed. The radiation-induced effects on charge collection are also studied via TCAD simulation, elaborated in Section 3. We conclude the radiation hardness of SUPIX-1 both from measurements and simulations in the last section.

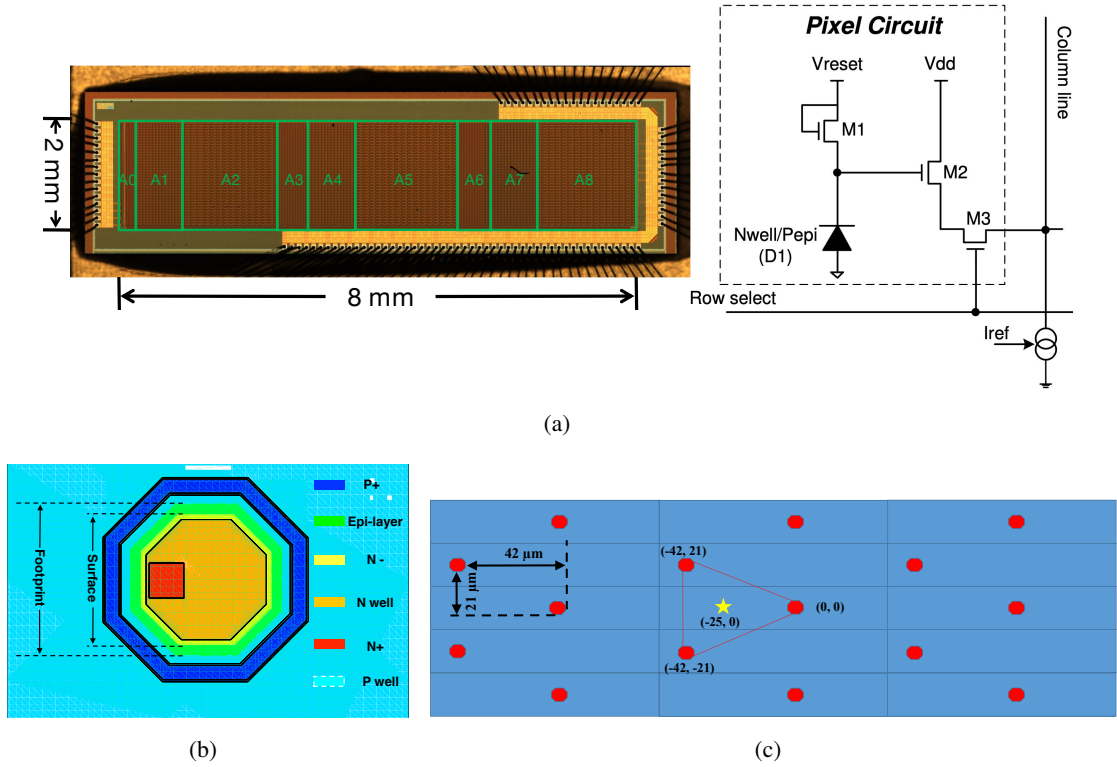


Figure 1: Design of the SUPIX-1 sensor: (a) a photograph and the schematic of in-pixel circuit, (b) the geometry of a sensor diode and (c) the staggered arrangement of diodes in sectors with the largest x-pitch.

2 Measurements with ^{55}Fe

The sensor is tested with the radioactive source of ^{55}Fe before and after irradiation. The test system and method are demonstrated in ref. [6].

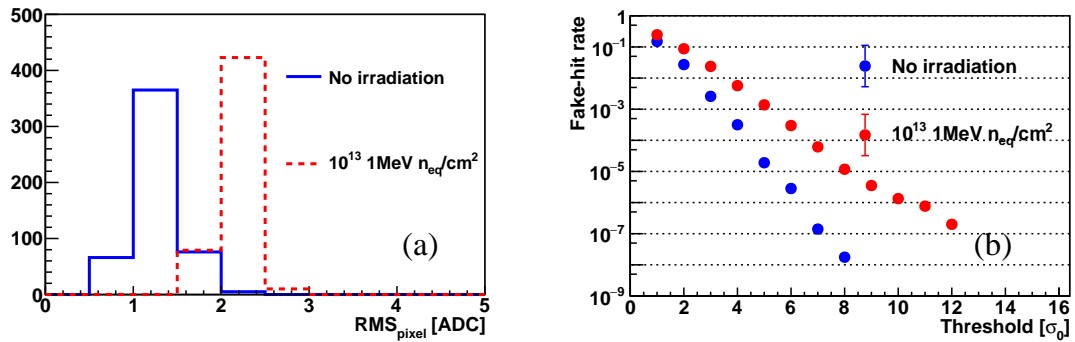


Figure 2: (a) Distributions of pixel-wise noise before (blue solid line) and after (red dashed line) irradiation. (b) The fake-hit rate versus the threshold before (blue bullet) and after (red bullet) irradiation. σ_0 is the RMS of the pixel output before irradiation.

Distributions of the fixed pattern noise before and after irradiation are shown in Figure 2(a). The mean of the $\text{RMS}_{\text{pixel}}$ increases from 1.3 to 2.1 ADC counts (ADC) after irradiation. As a result, the fake-hit rate as a function of trigger threshold, demonstrated in Figure 2(b), goes up by one to three orders of magnitude after irradiation.

2.1 The sensor gain calibration

The conversion gain (G) of the sensor is calibrated using the $k\text{-}\alpha$ (5.9 keV) soft X-ray of ^{55}Fe before and after irradiation. G is defined as

$$G = \frac{\text{ADC}}{Q}, \quad (2.1)$$

assuming 100% of CCE when the X-ray photons absorbed in the depleted region of a single diode. Q is the charge generated. 1640 electron-hole pairs can be liberated when a $k\text{-}\alpha$ photon is absorbed in silicon, assuming that 3.6 eV at room temperature is needed to create an electron-hole pair[7].

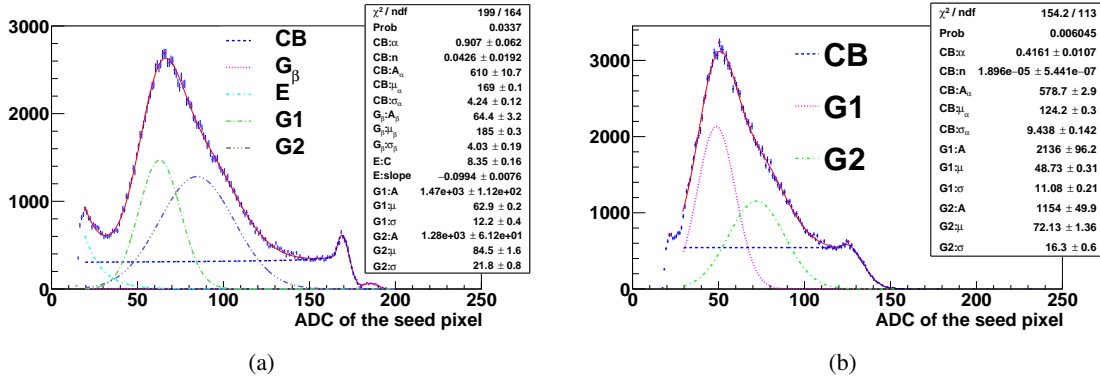


Figure 3: Distributions of seed-pixel ADC (a) before and (b) after 1×10^{13} 1 MeV $n_{\text{eq}}/\text{cm}^2$ neutron irradiation, together with full-spectrum fits.

The spectra of ^{55}Fe , reconstructed by seed pixels, before and after irradiation are shown in Figure 3(a) and (b), separately. Almost full spectra are well fitted by combinations of component functions. At the right end of the spectrum, the $k\text{-}\beta$ (6.5 keV) peak disappears in (b). A single crystal ball function (CB), instead of the combination of CB and Gaussian function (G_β) in (a), is applied to describe the full energy peak of $k\text{-}\alpha$. Peak with the highest amplitude (collection peak), contributed by the incident X-ray photons in the vicinity of the seed pixel, is well described by two Gaussian functions (G1 and G2) superposed with the tail of CB. The exponential function (E), describing the pedestal toward the left end of the spectrum in (a), fails in the fit in (b).

The $k\text{-}\alpha$ peak shifts toward left by 45 ADC, as a result of the increased diode capacitance after irradiation. The capacitance of a reversely biased diode (C) shown in Figure 7(b) can be estimated using the formula for parallel plate capacitor:

$$C = \epsilon_0 \epsilon_{\text{Si}} \frac{A}{d}, \quad (2.2)$$

where ϵ_0 and ϵ_{Si} are vacuum permittivity and relative permittivity of silicon, A and d are the area and depth of the depleted region. The radiation-induced decrease of d leads to the increase of C. Thus, the sensor output, Q/C , decreases.

Table 1: The geometrical parameters of SUPIX-1 sensor and the test results of sensor gains and ENC of respective sectors, 0 represents the sensor before irradiation while 10^{13} stands for the sensor after 1×10^{13} 1 MeV n_{eq}/cm^2 neutron irradiation.

| Sector | | A0 | A2 | A5 | A7 | A8 |
|-------------------------|-----------|-------------|-------------|-------------|-------------|-------------|
| Surface (μm^2) | | 8 | 8 | 12 | 20 | 20 |
| Footprint (μm^2) | | 11 | 11 | 18 | 44 | 50 |
| G (ADC/e) | 0 | 0.103±0.003 | 0.123±0.003 | 0.100±0.003 | 0.110±0.002 | 0.112±0.003 |
| | 10^{13} | 0.076±0.006 | 0.085±0.006 | 0.061±0.007 | 0.060±0.007 | 0.049±0.007 |
| ENC (e) | 0 | 13±3 | 12±2 | 13±3 | 12±4 | 12±2 |
| | 10^{13} | 28±3 | 27±3 | 42±6 | 50±6 | 70±10 |

The conversion gains calibrated with k- α peaks for all sectors are listed in Table 1. All sectors suffer considerable degradations after irradiation. The largest decrease of G, 56.3%, is found in A8 which has the biggest diode dimension. Corresponding decreases for A2 and A5 are 30.9% and 39.0% respectively. A7 which has the same diode surface area as A8 does but smaller diode footprint area, suffers less decrease of 45.5% than A8 does. Degradations on G show that bigger diode is more sensitive to the radiation-induced effects. The difference of decrease between A0 and A2 is less than 5%, indicating weak dependence on pixel pitch.

The fixed pattern noise in Figure 2(a) is transformed into ENC after G being calibrated. As listed in Table 1, for small diodes, increases of ENCs for A0 and A2 are 115% and 125% respectively after irradiation. For medium size diodes, A5 increases by 223%. A7 and A8, which has the largest diode surface area, suffer the increase of ENC over 300%. And the increase of A8 is 50% more than that of A7 due to the larger area of footprint.

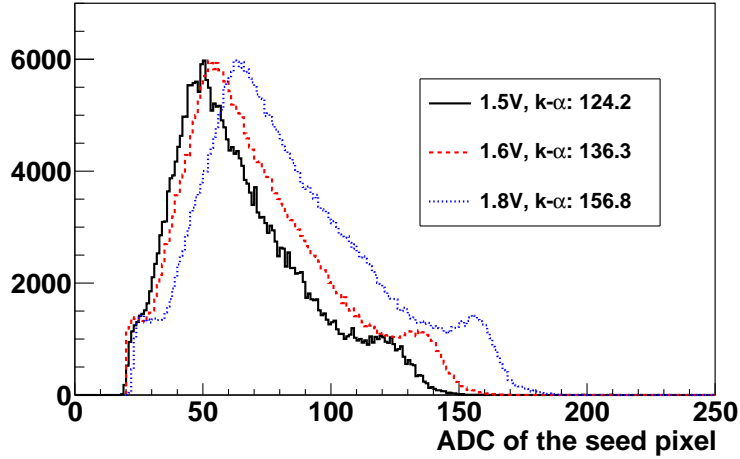


Figure 4: Distributions of seed-pixel ADC under various biased voltages.

The pixel-wise CCE SNR are defined in ref. [6]. Test results for all sectors before and after irradiation are summarized in Table 2. CCEs, for the same sector, are consistent within uncertainties before and after irradiation. However, SNRs suffer decreases after irradiation. Decreases on SNR

exhibit strong dependence on diode geometry. Bigger the diode is, larger gets the ENC after irradiation. Consequently, larger diodes suffer more decreases on SNR.

We have increased the biased voltage from 1.5 V (default) to 1.8 V (maximum allowed) to see the difference of sensor performance. The $k\alpha$ peak, A0 as an example, has a right-shift with the voltage going up, so as the collection peak, as shown in Figure 4. Correspondingly, the sensor gain increases from 0.076 ADC/e (1.5 V) to 0.096 ADC/e (1.8 V) and the ENC decreases from $28 e^-$ to $21 e^-$.

2.2 The cluster-wise sensor properties

Mostly, charge carriers ionized by incident photons of ^{55}Fe are collected by several pixels through thermal diffusions in the epitaxial layer, forming clusters. The cluster properties and the radiation-induced effects are studied with a self-developed reconstruction algorithm introduced in ref. [6]. In ref. [6], the clustering threshold for fired pixels, based on pixel SNR, is set to be 3.1 for less than one per mil of noise pixels leaked into the cluster. A new determination of the clustering threshold, shown in Figure 5, is developed in this work. Distributions of pixel SNR with (calibration run) and without (noise run) ^{55}Fe are shown in (a). Quantiles of the pixel SNR distribution in calibration run as a function of that in noise run are shown in (b). The function is not linear with slope of 1 any more when $\text{SNR} > 2.8$, which means the signal for X-ray of ^{55}Fe dominates. Thus, SNR of 2.8 is selected as the clustering threshold in this paper.

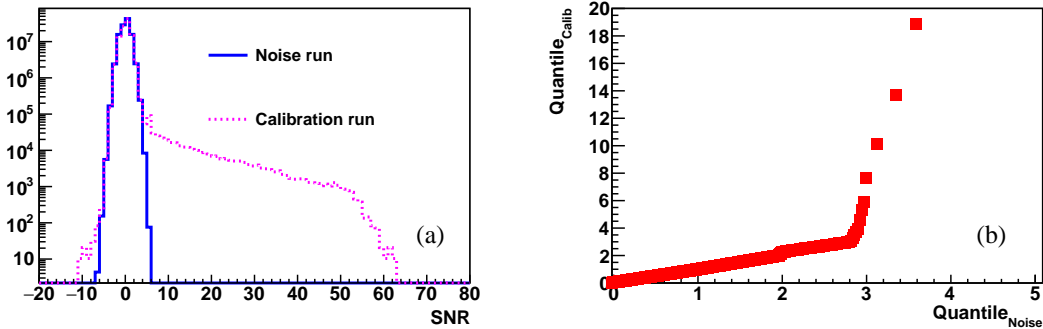


Figure 5: The determination of the clustering threshold after neutron irradiation: distributions of the pixel SNR with (calibration run) and without (noise run) ^{55}Fe , (b) quantiles of the pixel-wise SNR distribution in calibration run as a function of that in noise run.

The cluster properties before and after irradiation are demonstrated in Figure 6. The mean of the cluster size, shown in (a), decreases from 4.4 to 2.4 after irradiation, as a result of charge trapping. The cluster SNR, shown in (b), also decreases, but most of clusters have the SNR over 20. Distributions of the cluster ADC before and after irradiation are shown in (c) and (d) respectively, together with the distribution of seed-pixel ADC for comparison. The distributions are well fitted by Gaussian functions superposed a crystal ball function.

The cluster-wise CCE and SNR, defined in ref. [6], are measured for the irradiated sensor. Results along with that before irradiation are summarized in Table 2. Before irradiation, the cluster properties show weak dependence on geometrical configuration. On the one hand, the SNRs are consistent within uncertainties. On the other hand, variations of CCEs are within about 5% referring

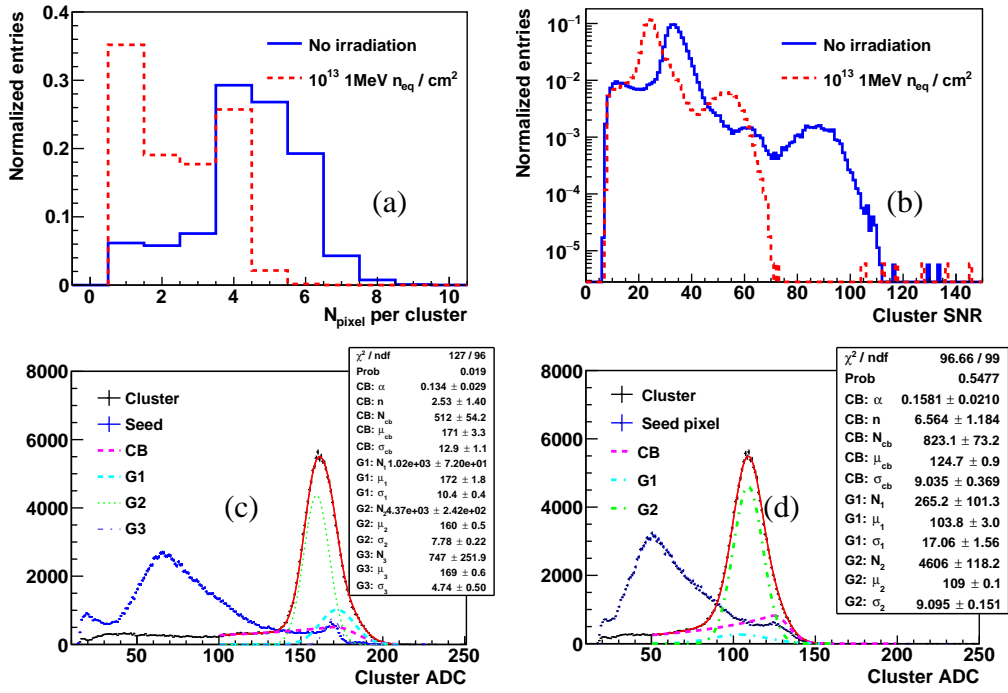


Figure 6: Variations of the cluster properties: (a) the cluster size and (b) the cluster SNR before (blue) and after (rad) irradiation, and the ADC sum of the cluster before (c) and after (d) irradiation.

Table 2: Geometrical parameters of the SUPIX-1 sensor and the test results with ^{55}Fe radioactive source, 0 represents the sensor before irradiation while 10^{13} stands for the sensor after the 1×10^{13} 1 MeV $n_{\text{eq}}/\text{cm}^2$ of the neutron irradiation.

| Sector | | A0 | A2 | A5 | A7 | A8 | |
|-------------------------------------|------------------|-----|----------------|----------------|----------------|----------------|----------------|
| Sensitive Area x (mm) | | 0.3 | 1.3 | 1.3 | 0.6 | 1.3 | |
| Sensitive Area y (mm) | | 1.3 | | | | | |
| Pixel Pitch x (μm) | | 21 | 84 | 84 | 42 | 84 | |
| Pixel Pitch y (μm) | | 21 | | | | | |
| Diode Surface (μm^2) | | 8 | 8 | 12 | 20 | 20 | |
| Diode Footprint (μm^2) | | 11 | 11 | 18 | 44 | 50 | |
| Pixel | 0 | CCE | 39.1 \pm 1.0 | 31.7 \pm 0.7 | 27.5 \pm 0.6 | 30.4 \pm 0.8 | 37.2 \pm 0.7 |
| | | SNR | 52 \pm 11 | 49 \pm 10 | 36 \pm 8 | 42 \pm 9 | 53 \pm 11 |
| | 10 ¹³ | CCE | 40.1 \pm 1.5 | 31.8 \pm 1.0 | 26.0 \pm 1.1 | 31.6 \pm 1.1 | 37.7 \pm 1.2 |
| | | SNR | 23 \pm 2 | 19 \pm 1 | 10 \pm 1 | 10 \pm 1 | 9 \pm 1 |
| Cluster | 0 | CCE | 95.6 \pm 0.5 | 90.3 \pm 0.4 | 93.8 \pm 0.5 | 96.8 \pm 0.4 | 92.4 \pm 0.6 |
| | | SNR | 36 \pm 3 | 33 \pm 2 | 32 \pm 2 | 36 \pm 3 | 36 \pm 3 |
| | 10 ¹³ | CCE | 89.0 \pm 1.0 | 75.2 \pm 0.9 | 73.9 \pm 1.5 | 90.6 \pm 1.7 | 73.2 \pm 1.7 |
| | | SNR | 22 \pm 2 | 19 \pm 2 | 12 \pm 2 | 14 \pm 2 | 10 \pm 2 |

to the CCE of A0. The decreases of CCE after irradiation show the significance of pixel pitch in charge collection. The decrease of CCE for A0 is less than 7% but 17% for A2. Variations of decreases among sectors with largest x-pitch are less than 5%. A7 has larger diode dimensions than A0 does and the pixel pitch of A7 is twice of A0's. A7 gets the similar decrease on CCE as A0 does. The decreases of SNR are apparent after irradiation for all sectors. The decreases of pixel-wise and cluster-wise SNR exhibit similar dependence on diode geometry.

3 TCAD simulations

The radiation-induced damage, under fluence of 1×10^{13} 1 MeV n_{eq}/cm^2 , on charge collection are studied via TCAD. Simulations are consisted of device construction and emulations of electric properties of devices with physics models.

The device construction consists of geometry definition and doping profile. 5×5 pixel matrixes with the same diode geometries and pixel arrangements in sectors measured are constructed. As an example, the top view of a 5×5 pixel matrix in A0 is shown in Figure 7(a), in which the X-Y co-ordinate of the diode at bottom-left is $(-42, -42)$ in the unit of μm , as a reference. The device is divided into small building blocks by doping concentration dependent meshing strategy, shown as black lines, for finite element analyses. With the limits of the CPU (Intel Core i7-6700 3.4 GHz) and the random access memory (48 GB DDR4), total vertices and elements of building blocks are controlled within 200 000 and 1 000 000 respectively. Additional volumes of silicon (green) with low doping concentration ($< 10^5 cm^{-3}$) are added to boundaries due to the reflective boundary conditions[8].

Figure 7(b) shows the doping concentration of a single diode in Y-Z plane. The doping concentration of phosphorus (boron) is higher, as the color of the doped area gets redder (bluer). The doping strategy of N-well (P-well) along Z axis is a combination of multiple Gaussian functions with peak concentrations ranging from $4.5 \times 10^{17} cm^{-3}$ to $5 \times 10^{19} cm^{-3}$. A reversely biased voltage of 1.5 V is applied on the N-well diode, forming the depleted region with the depth of $4.9 \mu m$, enclosed by the white lines in Figure 7(b). The thickness of the device is $200 \mu m$.

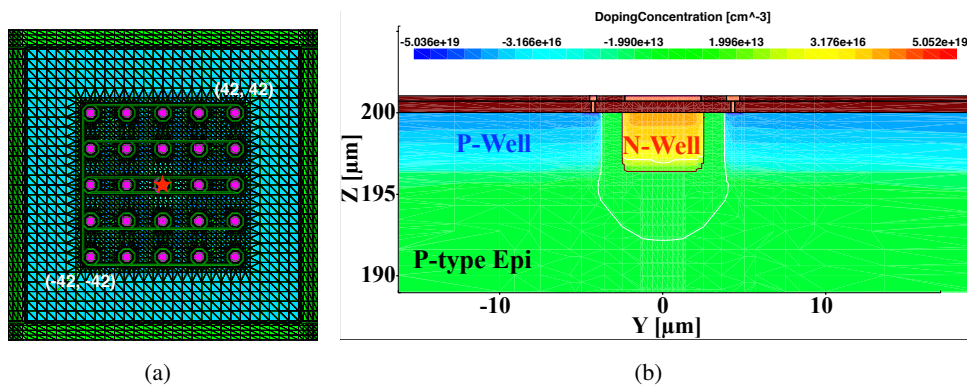


Figure 7: (a) the topview of a simulated device with 5×5 pixel array in A0 and (b) the doping profile of a single diode in Y-Z plane.

A heavy ion model is applied to simulate the charge generation of minimum ionizing particles (MIPs) in silicon. In the model, the linear energy transfer parameter is set to be 1.28×10^{-5} pC/ μm for the estimated most probable energy loss rate of 80 electron-hole pairs/ μm for MIPs in 200 μm silicon[7]. Simulation vary with the impinging positions of incident particles. Two typical cases are chosen for discussion. The first one is (0, 0) in X-Y plane (case 1), shown as the red star in Figure 7(a), on which a pixel diode is hit. The other one is complicated. Positions in case 2 for A0 and A7 are (10, 10) and (21, 10) respectively. They locate the center of four pixels. For sectors with x-pitch of 84 μm , (-25, 0) which is the center of 3 pixels, shown in Figure 1(c), is selected. The incident direction is along Z axis and the length of the track is 200 μm .

For bulk damage on the sensor, a three level radiation damage model is applied[9]. In this model, radiation induced traps are distributed on different energy levels, as listed in Table 3. E_c is the energy level of conduction band of silicon while E_v is for the valence band. σ_n (σ_p) is the cross-section between a trap and an electron (hole) and η is the introduction rate. The concentration of radiation induced traps (N_{traps}) is given by

$$N_{\text{traps}} = \eta \Phi_{\text{eq}}, \quad (3.1)$$

where Φ_{eq} is the neutron equivalent fluence.

Table 3: The parameters of three-level radiation damage model. E_c represents the energy level of conduction band while E_v is for the valence band. σ_n (σ_p) is the cross-section between a trap and an electrons (hole) and η is the introduction rate.

| Energy level | $\sigma_n(\text{cm}^{-2})$ | $\sigma_p(\text{cm}^{-2})$ | $\eta(\text{cm}^{-1})$ |
|-----------------|----------------------------|----------------------------|------------------------|
| $E_c - 0.42$ eV | 2.0×10^{-15} | 2.0×10^{-14} | 1.613 |
| $E_c - 0.46$ eV | 5.0×10^{-15} | 5.0×10^{-14} | 0.9 |
| $E_v + 0.42$ eV | 2.5×10^{-14} | 2.5×10^{-15} | 0.9 |

Simulated charge collections, as functions of pixels after descending orders of electrons collected, are presented in Figure 8. Charge collected for seed pixels ($N_{\text{pixel}} = 1$) are consistent before and after irradiation. For pixel matrix, case 2 has a large decrease of Charge collected than case 1 does. 90% of the charge collection are done within 5 pixels in case 1 and 10 in case2. Results for all sectors are summarized in Table 4. In case 1, Decreases of charge collected for seed pixels are within 7% after irradiation. Decreases for pixel matrixes are within 13%. A0 which has the smallest pixel pitch gets the smallest decrease, 6%. The decrease of A7 which has the medium size pixel pitch is 7%, close to that of A0. Variations of decreases for large pixel sectors with various diode geometries are within 3%. In case 2, all sectors suffer considerable loss on charge collection, over 48%, both for seed pixel and matrix except A0. The simulation indicates that diffusion length is the key point for the radiation induced signal loss. Longer the charge carriers diffuse, more possibly are they trapped by defects. Thus, small pixel pitch gains an edge on charge collection after irradiation. The test results are between typical cases simulated and are close to case1.

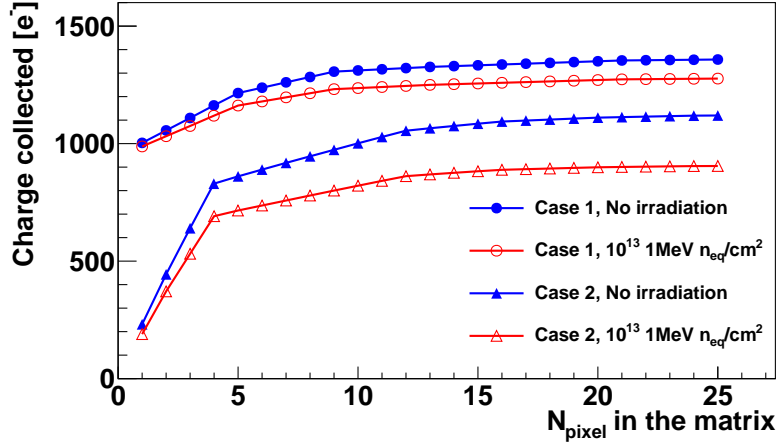


Figure 8: Simulated charge collections as functions of pixels in the matrix before (blue) and after (red) irradiation. Case 1 is represented by the marker of circle while case 2 is shown as triangle.

Table 4: Geometrical parameters of SUPIX-1 sensor, and the charge collection simulation before and after irradiation. See the text for explanation.

| Sector | | | A0 | A2 | A5 | A7 | A8 | |
|-------------------------------------|--|-------|--------|------|------|------|------|------|
| Pixel Pitch x (μm) | | | 21 | 84 | 84 | 42 | 84 | |
| Pixel Pitch y (μm) | | | 21 | | | | | |
| Diode Surface (μm^2) | | | 8 | 8 | 12 | 20 | 20 | |
| Diode Footprint (μm^2) | | | 11 | 11 | 18 | 44 | 50 | |
| Q (e) | 0 (1 MeV $n_{\text{eq}}/\text{cm}^2$) | Case1 | Seed | 1003 | 1117 | 1231 | 1235 | 1287 |
| | | | Matrix | 1358 | 1227 | 1321 | 1467 | 1463 |
| | | Case2 | Seed | 231 | 155 | 188 | 179 | 256 |
| | | | Matrix | 1120 | 521 | 636 | 821 | 748 |
| | 10 ¹³ (1 MeV $n_{\text{eq}}/\text{cm}^2$) | Case1 | Seed | 988 | 1040 | 1188 | 1201 | 1226 |
| | | | Matrix | 1276 | 1077 | 1202 | 1367 | 1303 |
| | | Case2 | Seed | 189 | 55 | 78 | 92 | 105 |
| | | | Matrix | 905 | 163 | 266 | 398 | 260 |

4 Conclusion

The radiation induced effects on SUPIX-1, a CMOS pixel sensor, under the fluence of 1×10^{13} 1 MeV $n_{\text{eq}}/\text{cm}^2$ are studied via by measurements with radioactive source of ^{55}Fe and TCAD simulations. In measurements, the sensor gain is calibrated using the $k\text{-}\alpha$ X-ray of ^{55}Fe . Then, the ENC and the pixel-wise CCE and SNR are obtained. The radiation-induced effects on properties of pixel clusters are studied with a preliminary clustering algorithm. A new determination of clustering threshold, based on the quantiles of the pixel-SNR distributions in noise run and calibration run, is developed. In simulations, two typical impinging positions of incident particles are selected and the corresponding charge collections in 5×5 pixel matrixes before and after irradiation are simulated.

The calibration of the sensor gain shows strong dependence on diode geometries. The larger diodes suffer more decreases of sensor gain after irradiation. Degradations on ENC show the similar dependence, so do the pixel-wise and cluster-wise SNR which are ENC related.

For radiation-induced effects on charge collection, the test results are between the typical cases in simulation, and are close to simulations in case 1. The tested decreases on pixel-wise CCEs are negligible for all sectors, consistent with the simulations in case 1. The measured decreases on cluster-wise CCE for A0 and A7 are similar and are less than that of large-pixel sectors, implying that large diode dimensions help on charge collection after irradiation with a constrained pixel pitch ($42\ \mu\text{m}$ in this work). The cluster-wise test results are also close to the simulations in case 1.

The test results demonstrate that SUPIX-1 sensor, suffering considerable loss of sensor performance especially on sensor gain and ENC, survives after neutron irradiation with fluence of $1 \times 10^{13}\ 1\ \text{MeV}\ n_{\text{eq}}/\text{cm}^2$. The pixels of all sectors keep almost the same CCE as that before irradiation and the effective SNR over 9. Besides, 70% of the CCE and 10 of the SNR, at least, are ensured for cluster. Though not as excellent as pixels in A0, the large pixels are also potential for tracking on CEPC. In large pixels, small diodes, like those in A2, are preferred after irradiation for the best performance on SNR.

Acknowledgments

This work has been supported by the National Natural Science Foundation of China (U1232202, U2032203 and 12075142), the Ministry of Science and Technology of China (2018YFA0404302) and Shandong Provincial Natural Science Foundation (ZR2020MA102).

References

- [1] The CEPC Study Group, “CEPC Conceptual Design Report: Volume 1 - Accelerator.” 2018, [arXiv:1809.00285](#).
- [2] The CEPC Study Group, “CEPC Conceptual Design Report: Volume 2 - Physics & Detector.” 2018, [arXiv:1811.10545](#).
- [3] L. Zhang, M. Fu, Y. Zhang et al., *Investigation of CMOS pixel sensor with $0.18\ \mu\text{m}$ CMOS technology for high-precision tracking detector*, *JINST* **12** (2017) C01011.
- [4] L. Rossi, P. Fischer, T. Rohe and N. Wermes, *Pixel Detectors: From Fundamentals to Applications*, Particle Acceleration and Detection, Springer-Verlag, Berlin (2006), [10.1007/3-540-28333-1](#).
- [5] ROSE collaboration, *Radiation hard silicon detectors developments by the RD48 (ROSE) Collaboration*, *Nucl. Instrum. Meth. A* **466** (2001) 308.
- [6] L. Li, L. Zhang, J. Dong, J. Liu and M. Wang, *Characterization of a CMOS pixel sensor for charged particle tracking*, *Journal of Instrumentation* **16** (2021) P12016.
- [7] PARTICLE DATA GROUP collaboration, *Review of Particle Physics*, *PTEP* **2020** (2020) 083C01.
- [8] G. Deptuch, *New Generation of Monolithic Active Pixel Sensors for Charged Particle Detection*, theses, Université Louis Pasteur - Strasbourg I, Sept., 2002.
- [9] M. Petasecca, F. Moscatelli, D. Passeri, G.U. Pignatell and C. Scarpello, *Numerical simulation of radiation damage effects in p-type silicon detectors*, *Nucl. Instrum. Meth. A* **563** (2006) 192.